Inorganic Chemistry

Article

pubs.acs.org/IC

Shape-, Size-, and Functional Group-Selective Binding of Small Organic Guests in a Paramagnetic Coordination Cage

Simon Turega, Martina Whitehead, Benjamin R. Hall, Anthony J. H. M. Meijer, Christopher A. Hunter,* and Michael D. Ward*

Department of Chemistry, University of Sheffield, Sheffield S3 7HF, United Kingdom

Supporting Information

ABSTRACT: The host–guest chemistry of the octanuclear cubic coordination cage $[Co_8L_{12}]^{16+}$ (where L is a bridging ligand containing two chelating pyrazolyl-pyridine units connected to a central naphthalene-1,5-diyl spacer via methylene "hinges") has been investigated in detail by ^{1}H NMR spectroscopy. The cage encloses a cavity of volume of ca. 400 Å^3, which is accessible through 4 Å diameter portals in the centers of the cube faces. The paramagnetism of the cage eliminates overlap of NMR signals by dispersing them over a range of ca. 200 ppm, making changes of specific signals easy to observe, and also results in large complexation-induced shifts of bound guests. The cage, in CD_3CN solution, acts as a remarkably size- and shape-selective host for small organic guests such as coumarin (K = 78 M^{-1}) and other bicyclic molecules of comparable size and shape such as isoquinoline-*N*-oxide (K = 2100 M^{-1}). Binding arises from two independent recognition elements, which have been separately quantified. These are (i) a polar component arising from interaction of the H-bond accepting O atom of the guest with a convergent group of CH protons inside the cavity that lie close to a *fac* tris-chelate metal center and are therefore in a region of high electrostatic potential; and (ii) an additional component arising from the second aromatic ring (aromatic/van der Waals interactions with the interior surface of the cage and/or solvophobic interactions). The strength of the first component varies linearly with the H-bond-accepting ability of the guest; the second component is fixed at approximately 10 kJ mol^{-1}. We have also used ^{1}H–^{1}H exchange spectroscopy (EXSY) experiments to analyze semiquantitatively two distinct dynamic processes, viz. movement of the guest into and out of the cavity and tumbling of the guest inside the host cavity. Depending on the size of the guest and the position of substituents, the rates of these processes can vary substantially, and the rates of processes that afford observable cross-peaks in EXSY spectra (e.g., between free and bound guest in some cases; between different conformers of a specific host·guest complex in others) can be narrowed down to a specific time window. Overall, the paramagnetism of the host cage has allowed an exceptionally detailed analysis of the kinetics and thermodynamics of its host–guest behavior.

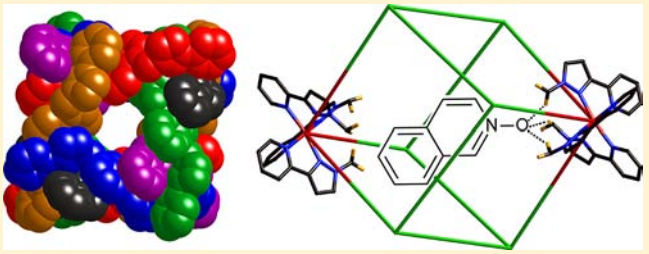

INTRODUCTION

Container molecules with central cavities that bind guests have been for a long time one of the most popular targets of study in supramolecular chemistry.[1,2] The two most common types of these are (i) metal-containing polyhedral coordination cages, which form by self-assembly of appropriate combinations of metal ions and bridging ligands,[1] and (ii) organic capsules such as cavitands and carcerands that may be covalently linked or may assemble via hydrogen-bonding interactions.[2]

As well as high selectivity of guest binding in some cases, useful consequences of guest binding can arise from remarkable changes in the reactivity of bound species. Paradigmatic examples include the photochemical synthesis and stabilization of cyclobutadiene inside an organic capsule,[3] stabilization of pyrophoric P_4 molecules in air when trapped inside a tetrahedral coordination cage,[4] alteration in the regioselectivity of Diels–Alder reactions due to the orientation imposed on the reacting pair of substrates in a confined space,[5] and the million-fold rate enhancement of a Nazarov cyclization arising from enzyme-like stabilization of the transition state.[6]

Most container molecules, whether they are hydrogen-bonded organic capsules or polyhedral coordination cages based on metal–ligand interactions, do not incorporate specific, directional recognition elements on their internal surfaces. Thus, the driving force for guest uptake is based on effects such as hydrophobic or van der Waals' interactions where guest selectivity is dictated largely by the shape/size effects encapsulated by Rebek's "55% rule".[2a,7] There are just a few examples of container molecules whose interiors are functionalized with specific groups to facilitate guest binding. Crowley and co-workers showed how a *cis*-platin molecule binds in the cavity of a small coordination cages as a result of specific hydrogen-bonding interactions with noncoordinated pyridyl groups in the ligand array whose N atoms are directed into the

Received: November 15, 2012
Published: January 9, 2013

   dx.doi.org/10.1021/ic302498t | Inorg. Chem. 2013, 52, 1122–1132

cavity to interact with the guest.[8] Fujita and co-workers have shown that a particular tripeptide sequence may be bound inside a cage cavity in preference to other tripeptides, partly because of specific H-bonding interactions with the interior surface of the cavity.[9] In general, we would expect that the presence of specific inwardly directed functional groups in a container molecule, which can interact with a guest in a geometrically specific manner, should facilitate highly selective molecular recognition of a complementary guest.

In this paper, we describe the host–guest chemistry of an octanuclear $[Co_8L_{12}]^{16+}$ paramagnetic coordination cage, which consists of a cubic array of metal ions with a bis-bidentate bridging ligand spanning each edge.[10] This is one of an extensive family of such cages based on bis(pyrazolyl-pyridine) bridging ligands that we have described in recent years.[1e,11] In a recent preliminary communication,[12] we reported how this cage binds coumarin in the central cavity with high selectivity as compared to a wide range of other potential guests of similar size and shape. In particular, potential guests that are nearly isostructural with coumarin but which lack the electronegative O atom (H-bond acceptor), such as 2-methylnaphthalene, showed no binding by NMR spectroscopy. On this basis, we hypothesized that binding of coumarin might involve CH···O hydrogen bonding between the internal surface of the cavity and the coumarin carbonyl group. In addition, the presence of small substitutents (methyl groups) at positions C^6 and C^7 on the coumarin skeleton also prevented binding, indicating a high degree of shape/size selectivity in addition to the functional group selectivity. We also demonstrated in this communication how the paramagnetism of the cage, arising from high-spin Co(II) ions, greatly facilitated NMR analysis of the host/guest binding by spreading the ^1H signals of the host out over a range of 200 ppm. This paramagnetism also resulted in very large complexation-induced shifts in the guest (of up to −12 ppm) as it enters a cavity surrounded by Co(II) ions.[12]

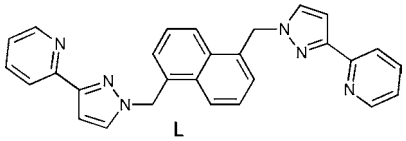

L

Following this initial characterization of a single host/guest complex for the cubic cage, we report here a much more detailed and extensive study of this behavior, with the properties of 14 complexes in three related series being examined. This has allowed two separate contributions to guest binding to be identified and quantified. Furthermore, exchange spectroscopy has been used to probe the kinetics of both the guest binding and the dynamic behavior of guests inside the cavity, allowing the rates of the two different exchange processes to be correlated with the steric properties of the guest. Molecular modeling calculations have been used to corroborate the conclusions arising from the spectroscopic studies. Overall, this work provides a very detailed analysis of both thermodynamics and kinetics of guest binding in a host cage, which displays high shape, size, and functional group selectivity for its guests. We note that the physical organic chemistry methods used herein are of widespread interest in the general study of self-assembled systems.[13]

RESULTS AND DISCUSSION

Structure of the Host Cage and Properties of Its Central Cavity. The crystal structures of $[Co_8L_{12}]^{16+}$ as its perchlorate and tetrafluoroborate salts have been reported earlier.[10,12] We briefly present here the structure of the newly characterized tetraphenylborate salt, which is very similar to these, but provides the opportunity to summarize those features of the cage structure that have turned out to be key in determining its molecular recognition properties (Figures 1 and 2). The approximately cubic array of Co(II) ions with Co···Co separations of either 10.84 or 11.42 Å along the edges is connected by 12 bis-bidentate ligands L, one spanning each edge. The space-filling view in Figure 1a shows the overall topology of the cage, the extensive aromatic stacking between ligand fragments around the periphery, which stabilizes the assembly, and the presence of portals to allow admission of

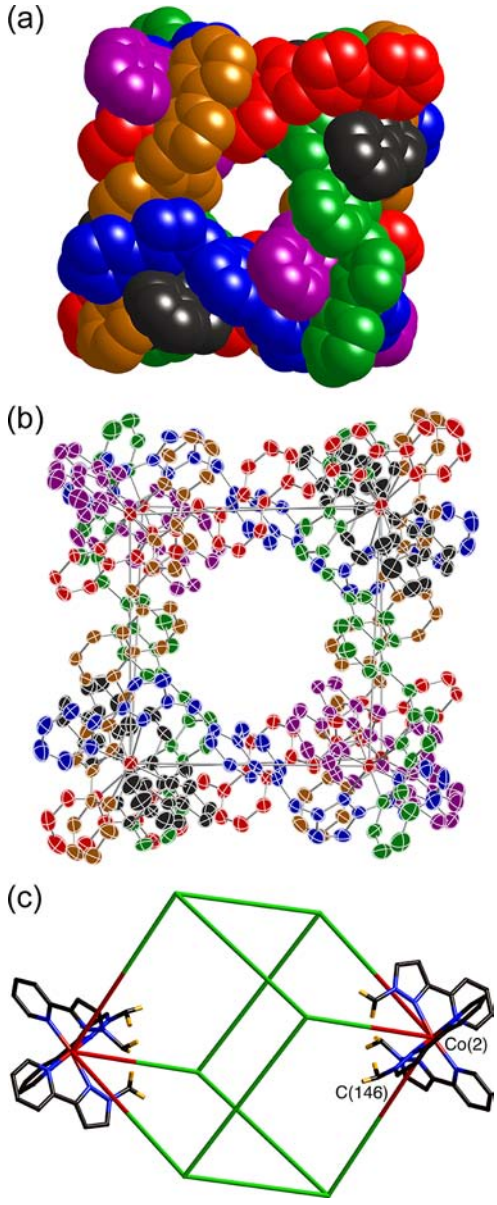

Figure 1. (a) Space-filling view of the cation of $[Co_8L_{12}](BPh_4)_{16}$ with ligands colored separately for clarity. (b) A thermal ellipsoid plot (40% probability level) of the cation from the same perspective and using the same coloring scheme. (c) Alternative view showing the coordinated ligand fragments around the *fac* tris-chelate Co(2) centers, especially the inwardly directed set of CH_2 protons (orange). The long diagonal connecting the two Co(2) centers is the C_3/S_6 axis.

dx.doi.org/10.1021/ic302498t | *Inorg. Chem.* 2013, 52, 1122–1132

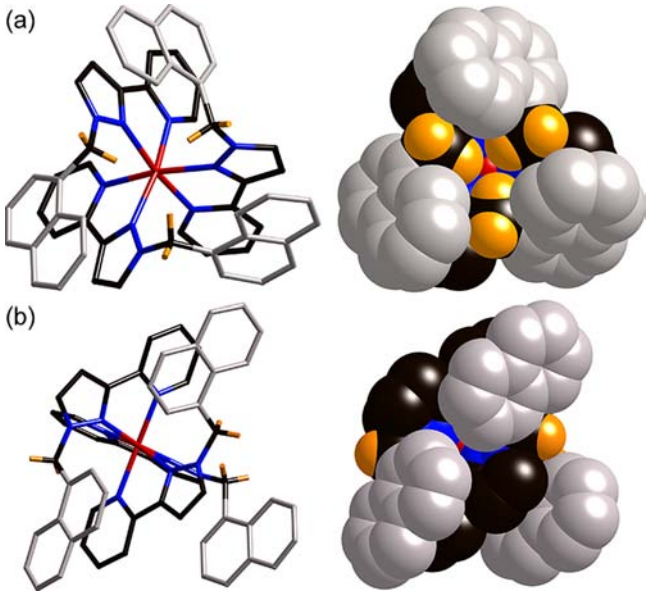

Figure 2. Wire-frame and space-filling views of (a) the *fac* [Co(2)] and (b) *mer* [Co(1)] tris-chelate metal centers in the cage cation of $[Co_8L_{12}](BPh_4)_{16}$. Naphthyl groups are in gray for clarity; the H atoms of the methylene groups are included (orange). In all cases, views are from the inside of the cavity looking outward. In a, the relatively exposed nature of the Co(II) center and the convergent set of methylene protons is clear as compared to the situation in b where the Co(II) center is less accessible.

guests to the cavity. The 2M:3L ratio is required to satisfy the principle of maximum site occupancy (Figure 1).[14]

Importantly, of the eight metal centers, six [all of the crystallographically equivalent Co(1) centers] have a *mer* tris-chelate coordination geometry, whereas the other two—a diagonally opposite pair of crystallographically equivalent Co(2) centers—have a *fac* tris-chelate coordination geometry. This gives the "cube" molecular S_6 symmetry with the two *fac* tris-chelate centers lying on the C_3/S_6 axis; the disposition of these two *fac tris*-chelate centers is emphasized in Figure 1c.

The presence of *fac* and *mer* tris-chelate metal centers at specific vertex sites differentiates regions within the pseudospherical cavity, and this turns out to be of fundamental importance for the host–guest chemistry described later. The environments around the *fac* [Co(2)] and *mer* [Co(1)] tris-chelate metal centers are shown in Figure 2, in both wire-frame and space-filling mode. It will be apparent from these views that the *fac* center is more "open" with the metal relatively exposed to the interior cavity, because of the orientation of the bulky naphthyl substituents, which all lie stacked with a chelating pyrazolyl-pyridine fragment (a recurrent feature of these complexes which contributes to their stability in solution).[1e,10,11] This leaves the three methylene groups with their protons oriented so as to define a pocket for CH···X interactions relatively close to the metal center. In contrast, at the *mer* tris-chelate center, the naphthyl groups are again oriented to stack with coordinated pyrazolyl-pyridine groups, but the lower local symmetry means that the metal center is protected by two of the naphthyl groups, and a guest in the cavity cannot get so close to the metal ion, nor is there a convergent network of H-bond donors.

The tetraphenylborate anions are located outside the cavity, with one lying over each of the six faces of the cube such that a phenyl ring docks into the "window" in the center of the face (Figure S1 in the Supporting Information)—a similar arrangement of anions located over the portals was observed for other salts of this cage.[10,12] The central cavity is apparently empty, although that is likely a crystallographic artifact of the "SQUEEZE" process that was used to eliminate regions of diffuse electron density from disordered solvent molecules. Importantly, however, any guest binding will not have to compete with anions that might otherwise occupy this cationic cavity.

The effect of the different *fac* and *mer* tris-chelate sites on the nature of the cavity is further illustrated by a molecular electrostatic surface potential map (Figure 3), calculated based

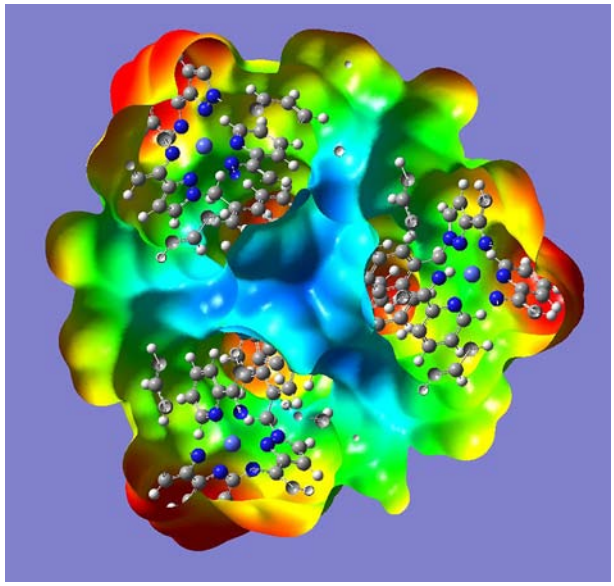

Figure 3. Cutaway view of the molecular electrostatic potential surface of the complex cation of $[Co_8L_{12}](BPh_4)_{16}$, looking up through the central cavity toward a *fac* tris-chelate vertex. Potential values range from +0.81 atomic units (blue) to +0.5 (red).

on the coordinates of the cage cation from the crystal structure. This clearly shows that the regions of highest electrostatic potential that are accessible to a guest (in blue) are precisely those pockets close to the two *fac* tris-chelate metal centers that are shown in Figure 1a.

The pseudospherical central cavity has a volume of 407 Å^3 (Swiss-PdbViewer 4.0.1); six round portals, one on each face of the cube, provide access to this cavity (Figure 1a). Space-filling models indicate that the cross-section of each portal is ca. 4 Å, which provides sufficient space for a molecular guest to enter the cage whose interior surface is lined with CH groups from the methylene groups and aromatic rings of the ligands. The aromatic rings of the ligands around the cavity interior surface are stacked with one another such that there are no exposed ligand surfaces available to participate in π-stacking interactions with aromatic guests. Rather, guest molecules can only interact with the ligands via van der Waals' interactions and weak polar interactions with the CH groups, with the most obvious sites for such polar interactions being close to the two *fac* tris-chelate vertices for both steric (Figure 2) and electronic (Figure 3) reasons.

Importantly, the paramagnetism of the high-spin Co(II) ions spreads out the 44 independent ^{1}H signals in the cage[11b,15]—arising from two independent ligand environments with no internal symmetry[10]—over the range −100 to +120 ppm.

dx.doi.org/10.1021/ic302498t | *Inorg. Chem.* 2013, 52, 1122–1132

Partial assignment is possible based on correlation of the T_1 values for these signals with the $[\Sigma(r_{H-Co})^{-6}]^{-1}$ distances for that proton (taken from crystallographic data);[15] see Table S1 in the Supporting Information for the measured T_1 values for all of the individually resolved ^{1}H NMR signals, as well as the $[\Sigma(r_{H-Co})^{-6}\ ]^{-1}$ values for each independent proton. The correlation between these has allowed complete assignment of the ^{1}H NMR spectra of smaller high-symmetry cages,[11b] but in the current case, the large number of signals with T_1 values that are comparable within experimental uncertainty means that unambiguous assignments are not possible. However, many ^{1}H signals can be assigned in this way, and those are indicated in Table S1 in the Supporting Information.

The ^{1}H NMR spectrum of the cage does not change with time, indicating its long-term stability—an essential prerequisite for meaningful host/guest studies. While cages of this nature are generally highly kinetically stable,[16a] we have observed in one case slow (days/weeks) rearrangement of one cage to another in solution.[11a] However, this is not an issue in this work with $[Co_8L_{12}]^{16+}$ salts.

Binding of Coumarin and Identification of Two Independent Recognition Elements in a Related Series of Isostructural Guests. Binding studies on potential guests were carried out using ^{1}H NMR spectroscopy in CD_3CN using the tetrafluoroborate salt of the cage. The polarity of this solvent reduces any competition with the BF_4^- counterion for the binding site. Guest binding was assayed using a 0.2 mM solution of the cage in CD_3CN, with sufficient guest added to make the guest concentration 50 mM.

On the basis of Rebek's "55%" rule,[7] the optimal volume of a guest for this cage is expected to be 224 Å^3. Initially, therefore, we tested a range of 19 potential guests **1**−**19** (see Figure S2 in the Supporting Information for structural formulas) of around this size, with the smallest being phenol (**6**, 88 Å^3) and the largest being *N*,*N*-dibutyl-benzenesulfonamide (**5**, 267 Å^3). As reported in the initial communication,[12] coumarin (**19**) was the only guest to show binding, with the guest in slow exchange such that separate signals for free host and the host/coumarin complex were observed. Integration of signals for free host and the host/coumarin complex at different concentrations of coumarin allowed determination of the association constant (K = 78 ± 20 M^{-1}).[12]

We have examined the cage·**19** complex in some detail. 1D GOESY and 2D EXSY experiments (Figure 4) could be used to observe excitation exchange between the signals of free **19**, and some of the new signals in the −6 to +4 ppm region of the ^{1}H NMR spectrum that appear during the titration can be ascribed to bound **19**. This allows signals for the free and the bound guest to be correlated: for example, the two vinylic protons (signals A and B in Figure 4) are clearly resolved in both free **19** and the complex $[Co_8L_{12}][BF_4]_{16}$·**19**, with signal A undergoing a complexation-induced change in chemical shift of ca. −12 ppm, from +6.4 (free) to −5.8 ppm (bound) (see Tables S2 and S3 in the Supporting Information for a full list of complexation-induced shifts for both host and guest in the complex $[Co_8L_{12}][BF_4]_{16}$·**19**). The signals due to the aromatic ring protons of free **19**, which occur in two overlapping pairs (C/D and E/F), also become substantially separated when in the paramagnetic cavity. Three new signals for bound **19** can be identified at 3.36, −0.33, and −0.54 ppm (E, F, and C, respectively); the fourth aromatic ring signal (D) for bound **19** is at 1.90 ppm and is obscured by solvent peaks but could be identified in the 1D GOESY experiment by its cross-peak. We

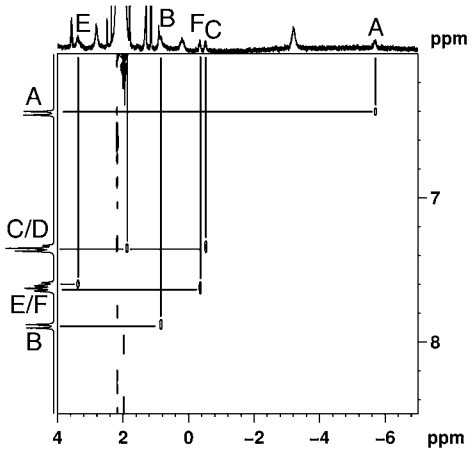

Figure 4. Observation of bound guest/free guest exchange. Partial 400 MHz 2D ^{1}H−^{1}H EXSY NMR spectrum (mixing time, 50 ms) recorded in d_3-acetonitrile at 298 K showing cross-peaks due to chemical exchange between free **19** (vertical axis) and the complex $[Co_8L_{12}][BF_4]_{16}$·**19** (horizontal axis). Concentrations: $[Co_8L_{12}]$-$[BF_4]_{16}$, 0.2 mM; **19**, 50 mM. The signal for proton D at +1.90 ppm in bound **19** is not visible as it is obscured by signals from residual protonated solvent, but the cross-peak is clearly visible, and this was confirmed by selective 1D GOESY experiments.

also note that a variable temperature series of ^{1}H NMR spectra revealed temperature-dependent changes in chemical shift ($\Delta\delta$ > 2 ppm between 271 and 309 K) for signals of bound **19** but not in the signals for free **19**, demonstrating the magnetic influence of the Co(II) ions on the ^{1}H signals for bound **19** (Figure S3 in the Supporting Information).

The large complexation-induced changes in chemical shifts in the guest arising from the paramagnetism of the host (Table S3 in the Supporting Information) facilitate identification of signals for the bound guest but also preclude conventional analysis in terms of the changes to be expected associated with H-bonding, π-stacking, and so on. In addition to substantial shifts of the guest on binding, smaller shifts of up to ca. 2 ppm were also observed in some of the host protons when the guest binds (Tables S2 and S4 in the Supporting Information). These $\Delta\delta$ values observed for the host signals are smaller than those for the guest signals as the host cage is already paramagnetic, and the additional shifts are only those arising from additional interactions with the diamagnetic guest.

Given that many potential guests that we evaluated from the initial set of 19 guest candidates showed no binding despite having very similar sizes and shapes to **19** [e.g., 2-methylnaphthalene (**17**) and 2-hydroxynaphthalene (**16**)], the selectivity for binding coumarin must depend on some specific recognition process. The only functional group in **19** that is different from those in **16** and **17** and which could make specific interactions with the interior of the cage is the carbonyl oxygen, which could act as an H-bond acceptor.

On this basis, we hypothesized[12] that the carbonyl oxygen of **19** might be acting as an H-bond acceptor. We have noted before that two other structurally characterized cages of this series[1e] exhibit multiple short CH···X contacts between anionic guests and the internal surface of the host, in particular the convergent array of inwardly directed CH_2 protons around a *fac* tris-chelate vertex (Figure 1b).[16] Indeed, $[Co_8L_{12}]X_{16}$ (X = ClO_4 or BF_4) both contain in their crystal structures solvent molecules in the cavity—MeOH and water, respectively—which show similar short contacts with the CH_2 groups around

dx.doi.org/10.1021/ic302498t | Inorg. Chem. 2013, 52, 1122−1132

the *fac* tris-chelate vertices.[12] As the calculation described earlier shows (Figure 3), these are the regions where electron-rich guests can approach the electropositive metal centers most closely, that is, where the electrostatic potential of the cavity is most positive.

We therefore examined as guests molecules **20**–**23** (Figure 5), which are isostructural with coumarin (**19**) but in which the

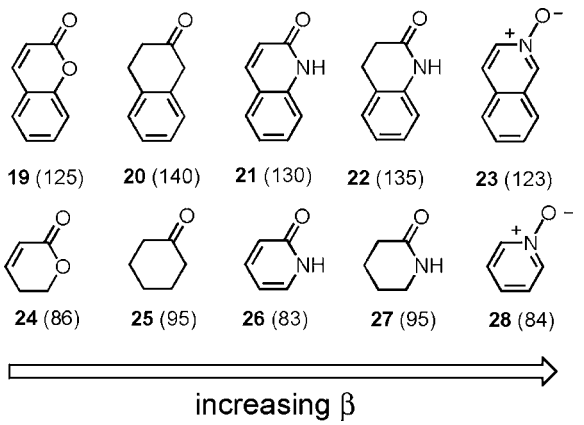

Figure 5. Two series of isostructural guests in which the H-bond acceptor ability of the oxygen atom (β parameter) is systematically varied. The numbers in parentheses are molecular volumes (Å^3).

H-bond accepting ability of the carbonyl oxygen atom, as encapsulated in its β value,[17] varies. The partial ^{1}H NMR spectra in Figure 6 show that all four additional guests showed slow-exchange binding with the host cage, resulting in separate sets of signals for free and bound host.

With guests **19** and **20**, each signal for the free host was replaced by one new signal for the host–guest complex (Figure 6, spectra b and c), indicating that, although guest exchange in and out of the cavity is slow on the NMR timescale, the host–guest complex retains its S_6 symmetry. This means that tumbling of the guest inside the host cavity must be fast on the

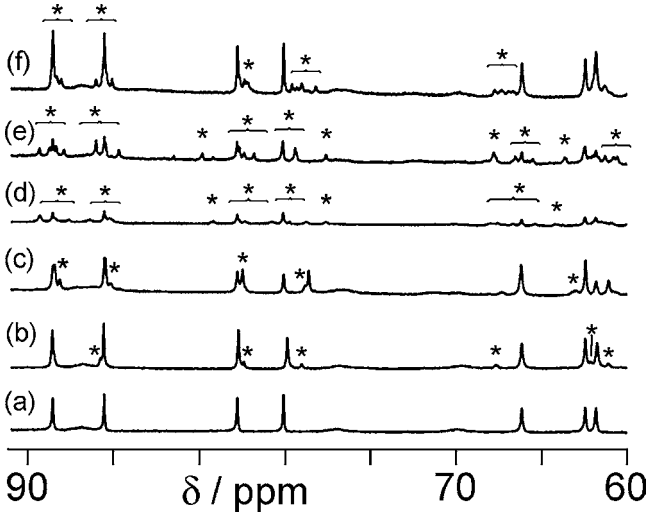

Figure 6. Partial 400 MHz ^{1}H NMR spectra recorded in d_3-acetonitrile at 298 K showing changes in some of the cage signals on addition of guests **19**–**23**. Signals due to the host–guest complexes are marked with an asterisk. The concentration of $[Co_8L_{12}][BF_4]_{16}$ is 0.2 mM; (a) no guest, (b) **19** = 14 mM, (c) **20** = 52 mM, (d) **21** = 1.3 mM, (e) **22** = 2.4 mM, and (f) **23** = 0.5 mM.

NMR timescale. In contrast, with guests **21**, **22**, and **23**, each signal for the free host was replaced by multiple signals for the host–guest complex (Figure 6, spectra d–f), indicating that not only is the in–out exchange process slow, but tumbling of the guest *within* the cavity is also slow on the NMR timescale, and this reduces the symmetry of the host cage. We return to this point in more detail in the next section when kinetics of these exchange processes are discussed; for the rest of this section, we focus on the thermodynamics of, and factors responsible for, guest binding.

Integration of signals for free and bound host at different guest concentrations (cf. Figure 6) allowed determination of association constants, and these are summarized in Table 1.

Table 1. Association Constants for the Formation of Complexes Between $[Co_{12}L_{18}][BF_4]_{16}$ and Guests 19–23 (CD_3CN, 298 K)

guest	β^a	K (M^{-1})	ΔG (kJ mol^{-1})
19	5.3	78 ± 20	−10.8 ± 0.6
20	5.3	28 ± 4	−8.3 ± 0.4
21	8.3	600 ± 90	−15.9 ± 0.4
22	8.3	880 ± 300	−16.8 ± 0.8
23	9.8	2100 ± 700	−19.0 ± 0.8

[a]From refs 17a–c.

The range of values spans 2 orders of magnitude and shows a clear trend of increasing association constant with increasing H-bond acceptor ability β for the guest, providing strong support for the hypothesis that a specific H-bonding interaction is important for guest binding. Isoquinoline-*N*-oxide (**23**), which is the best H-bond acceptor, makes the most stable complex (K = 2100 M^{-1}), and β-tetralone (**20**), which is the weakest H-bond acceptor, makes the least stable complex (K = 28 M^{-1}).

The free energies of complexation ($\Delta G°$) determined from the association constants in Table 1 show a linear correlation with the H-bond acceptor parameters of the guest (Figure 7). Equation 1 shows the relationship between the free energy contribution of an H-bond to complex stability ($\Delta\Delta G°$) and the H-bonding properties of the solutes (α and β) and solvent (α_S and β_S).

$$\Delta\Delta G° = -(\alpha - \alpha_S)(\beta - \beta_S) \quad (1)$$

If the cage behaves as a simple H-bond donor, and all guests interact in the same way, then for a series of different guests in the same solvent, eq 1 can be written as eq 2, where c and c' are constants.

$$\Delta\Delta G° = c\beta + c' \quad (2)$$

In other words, $\Delta\Delta G°$ should be linearly related to the guest β value as is observed in Figure 7. Moreover, eqs 1 and 2 show that the slope of the correlation in Figure 7 can be used to estimate an effective H-bond donor parameter for the host, the parameter α. The slope of the straight line for guests **19**–**23** in Figure 7 is 2.4, which implies that $\alpha \approx 4.1$ for the cage (as α_S for acetonitrile is 1.7). The binding pocket at the *fac* tris-chelate vertex of the cube therefore provides an interaction with H-bond acceptors that is comparable to what would be provided by a strong H-bond donor like phenol. The only H-bond donors on the cage interior are CH groups, and although the cage might make three simultaneous CH···O interactions at an H-bond acceptor site (see Figures 1c and 2a), the interactions with the guest will be strengthened by the proximity of these H-

dx.doi.org/10.1021/ic302498t | *Inorg. Chem.* 2013, 52, 1122–1132

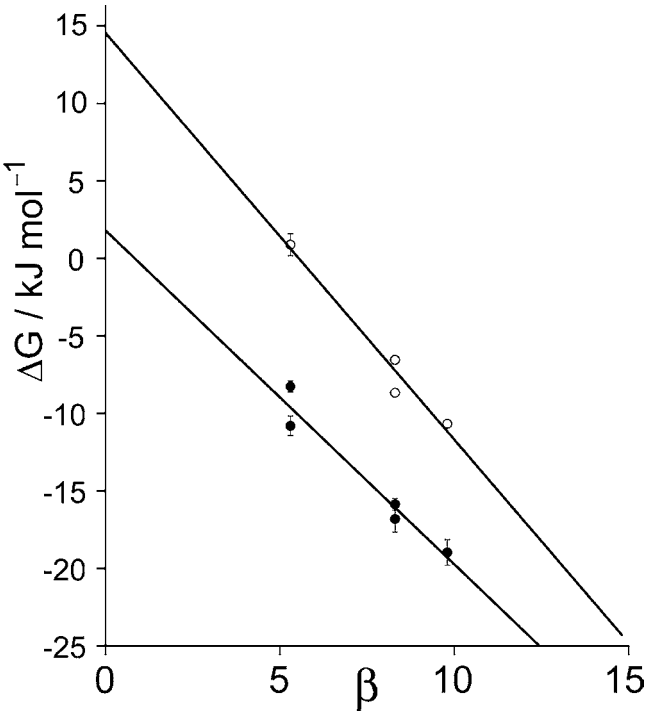

Figure 7. Plot of H-bond acceptor parameter (β) vs ΔG for complex formation for bicyclic guests **19**–**23** (black circles) and monocyclic guests **24**–**28** (hollow circles). Best fit straight lines are shown. Error bars for the ΔG values are included (see Tables 1 and 2); where these are not visible, it is because they are less than the height of the marker.

bonds to the *fac* tris-chelated Co^{2+} ions in the cage cavity, cf. the electrostatic potential map (Figure 3).

These results imply that guest binding could simply be due to interactions at a single polar binding site. To test this, we investigated monocyclic compounds **24**–**28** (Figure 5), which contain the same H-bond acceptor groups as **19**–**23** but which lack the second aromatic ring and are too small to fill the cavity. ^{1}H NMR titrations showed that, apart from **25** (cyclohexanone), these guests all bind to the cage and are in fast exchange in every case. Association constants were measured by fitting the changes in host chemical shift as a function of guest concentration to a 1:1 binding isotherm. The results are shown in Table 2.

Table 2. Association Constants for the Formation of Complexes Between $[Co_{12}L_{18}][BF_4]_{16}$ and Guests 24–28 (CD_3CN, 298 K)

guest	β^a	K (M^{-1})	ΔG (kJ mol^{-1})
24	5.3	0.7 ± 0.2	+0.9 ± 0.7
25	5.3	*b*	*b*
26	8.3	33 ± 1	−8.7 ± 0.1
27	8.3	14 ± 1	−6.5 ± 0.2
28	9.0	74 ± 7	−10.7 ± 0.2

[a]From refs 17a–c. [b]Binding too low to measure.

The association constant for each monocyclic guest is in every case weaker than for the analogous bicyclic guest with the same H-bonding group. For example, the association constant of the complex with an *N*-oxide guest decreased from 2100 M^{-1} with the bicyclic guest **23** to 74 M^{-1} with the related monocyclic guest **28**, and all other pairs display the same pattern. However, the H-bonding recognition element is still clearly operative, as the relative binding strengths of the monocyclic guests still correlate with the H-bond acceptor parameter (β).[17] The relationship between the free energy change on complexation ΔG and β for the monocyclic guests shown in Figure 7 is again linear and almost parallel with the line for the bicyclic guests; the slope of 2.9 implies an α value of 4–5 for the cage, very similar to that derived using the association constants of the bicyclic guests. However, the values of ΔG are consistently about 10 kJ mol^{-1} less favorable for the monocyclic guests, which indicates that the aromatic ring is not "innocent" but contributes to binding via weak interactions such as van der Waals' and CH···π interactions with the cage interior; solvophobic effects from this substituent may also contribute. Thus, we can observe and quantify from the data in Figure 7 *two separate components to guest binding*: a hydrogen-bonding component, whose magnitude varies with the β parameter of the guest, and an additional fixed contribution of ca. 10 kJ mol^{-1} from the second aromatic ring of the bicyclic guests.

A molecular mechanics-based model provides further confirmation of our hypothesis. We took the coordinates of the atoms in the complex cage cation from a crystal structure and constrained them, treating the cage as a rigid unit. A molecule of **19** was placed inside the cavity, and a molecular mechanics-based energy minimization was run. This was repeated multiple times from different guest starting positions. The energy-minimized structure found most commonly (Figure 8) shows the coumarin carbonyl group to be directed toward one of the two *fac* tris-chelate metal vertices such that it forms close contacts indicative of CH···O hydrogen bonds with the inwardly directed H atom from each of the three CH_2 groups, which define a binding pocket, with H···O distances of 2.76 Å. This is exactly consistent with the H-bond accepting O atom occupying the region of highest electrostatic potential that

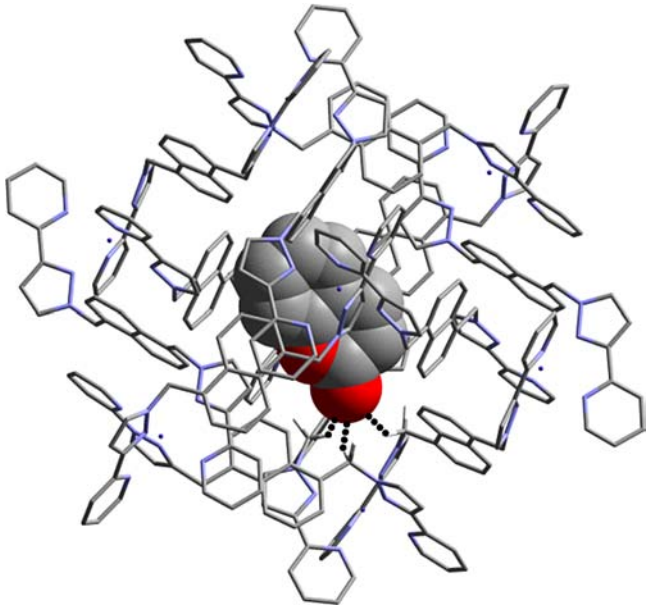

Figure 8. Calculated (molecular mechanics) structure of the complex between host cage and guest **19**. The host is shown in wire-frame view, and the guest is in space-filling view; H-bonds between methylene C–H groups of the host and the guest carbonyl are shown by black dots.

dx.doi.org/10.1021/ic302498t | *Inorg. Chem.* 2013, 52, 1122–1132

is sterically accessible in the cavity (Figure 3); that is, this electron-rich atom is lying as close as it can to a Co(II) ion.

Shape/Size Selectivity of Substituted Coumarins as Guests, and Their Dynamic Behavior Inside the Cavity. We noted above that there is clearly a high degree of shape and size selectivity associated with guest binding in the host cavity. In addition, we also noted that in some cases complex formation is associated with the appearance of multiple signals in the complex where there was a single signal in the free host; that is, the complex is desymmetrized due to slow tumbling of the guest in the cavity on the NMR timescale. Obviously, the shape and size of the guest affects the thermodynamics of guest binding, but it also affects the kinetic behavior of two different exchange processes, viz. in/out guest exchange, and tumbling within the cavity, and these can be partially quantified using EXSY NMR spectroscopy if their timescales fall within the temporal window of the EXSY experiment. In this section, we investigate these issues using a series of coumarins with different substitution patterns; Figure 9 shows the series of

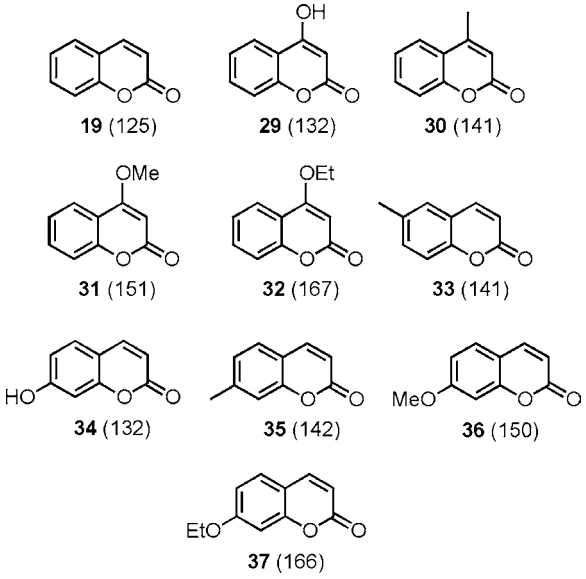

Figure 9. Substituted coumarins used to investigate the size/shape requirements for guest binding. Molecular volumes (Å^3) are in parentheses.

potential guests studied to investigate this shape/size selectivity in guest binding. 4-Methylcoumarin (**30**) is not commercially available but was prepared from a literature procedure.[18]

First, we look at binding constants. Partial paramagnetic ^{1}H NMR spectra from titrations of these substituted coumarins into a solution of the cage complex in d_3-acetonitrile are shown in Figure 10. Compounds **29**, **30**, **31**, and **34** all form complexes with the cage, but the other compounds do not. We assume that **32**, **33**, **35**, **36**, and **37** are all too large or the wrong shape to fit inside the cavity. Thus, the cage can tolerate substituents at the C^4 position of coumarin that are smaller than an ethoxy group. Small substituents are tolerated at the C^8 position (hydroxy, but not methyl or larger), and C^7 must be unsubstituted, as shown in the sketch in Figure 11.

This sensitivity of guest binding to the position of the substituents can be understood with reference to molecular models, which shows that substituents in the C^4-position are relatively unhindered as they are directed toward a portal in the center of one of the faces. Figure 12 shows a view of part of the

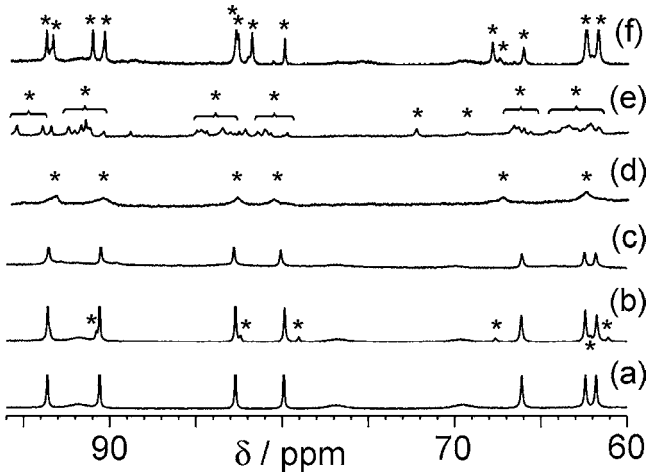

Figure 10. Partial 400 MHz ^{1}H NMR spectra recorded in d_3-acetonitrile at 298 K showing changes in some of the cage signals on addition of guests **19**, **29**, **30**, **31**, and **34**. Signals due to the host–guest complexes are marked with an asterisk. Concentration of $[Co_8L_{12}][BF_4]_{16}$ is 0.3 mM; (a) no guest, (b) **19** = 14 mM, and (c) **34** = 18 mM. Concentration of $[Co_8L_{12}][BF_4]_{16}$ is 0.15 mM; (d) **29** = 34 mM, (e) **31** = 31 mM, and (f) **30** = 7.2 mM.

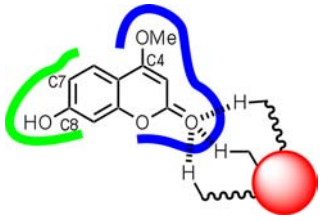

Figure 11. Sketch showing the binding of a coumarin derivative and the largest substituents allowed at the C^4, C^7, and C^8 positions.

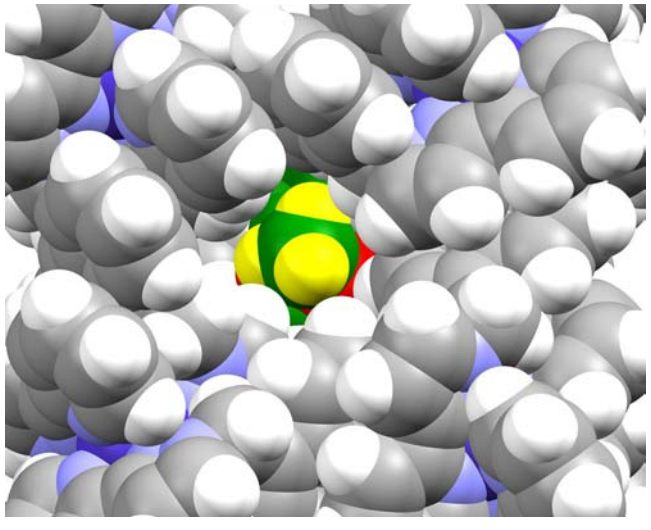

Figure 12. Partial view of the calculated (molecular mechanics) structure of the complex between the host cage and the guest **31**, viewed from the exterior of the cage, showing the "docking" of the MeO substituent (C in green, H in yellow, and O in red) in one of the portals.

energy-minimized structure of the complex with **31**, which is very similar to that shown in Figure 8 for coumarin but with the C^4 methoxy substituent of the guest (green/yellow) occupying a window in one the cage faces and therefore being relatively

dx.doi.org/10.1021/ic302498t | Inorg. Chem. 2013, 52, 1122–1132

unhindered. Calculations of the host/guest structures of the complexes with **19** (Figure 8) and **30** and **31** (Figures S4 and S5 in the Supporting Information) all gave very similar results. In contrast, the calculation using guest **32**, for which a complex is not observed experimentally due to the additional bulk of the C^4 substituent, failed to minimize to a well-defined structure with H-bonds between the carbonyl group and the CH_2 groups of the *fac* tris-chelate metal vertices.

Table 3. Association Constants for the Formation of Complexes Between $[Co_{12}L_{18}][BF_4]_{16}$ and Substituted Coumarin Guests (CD_3CN, 298 K)

guest	K (M^{-1})
19	78 ± 20
29[a]	63 ± 6
30	260 ± 90
31	91 ± 8
34[a]	53 ± 30

[a]Measured using fast exchange $\Delta\delta$s.

Table 3 shows the association constants measured from the ^{1}H NMR titrations (Figure 10) for those coumarins that do bind. The presence of substituents that are small enough to fit into the cage clearly has little impact on the magnitude of the observed association constants, which indicates that they do not make additional interactions with the walls of the cavity.

Next, we look at kinetic aspects of guest uptake and guest tumbling inside the cavity. Starting with our initial complex with coumarin (**19**), the use of a phase-sensitive NOSY sequence to run ^{1}H−^{1}H EXSY NMR experiments allows observation of exchange cross-peaks between free and bound *host* signals in $[Co_8L_{12}][BF_4]_{16}$ and $[Co_8L_{12}][BF_4]_{16}$·**19** (Figure 13). This is in addition to the exchange between free and bound *guest* signals shown in Figure 4.

We note here that the short T_1 relaxation times arising from the paramagnetism make many NMR experiments, including exchange spectroscopy, difficult. Exchange peaks could only be observed for those cage signals that had T_1 times longer than about 30 ms, allowing the observation of exchange peaks for 14 of the 44 independent cage signals (e.g., the four pairs of free cage/bound cage signals included in Figure 13). In addition, the EXSY experiment has a limited kinetic range, and the observed rate of exchange must be between 1 and 40 s^{-1} to observe a cross-peak. Thus, we have a temporal "window" within which the rate of the exchange process under observation can be placed by this technique. With guest **19**, we can place the timescale for guest exchange into/out of the cavity within this window. Tumbling of **19** in the cavity is of course fast on the NMR chemical shift timescale, as the host·**19** complex retains the symmetry of the free host.

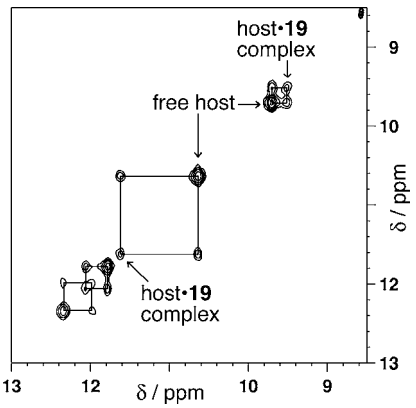

Figure 13. Observation of bound host/free host exchange. Partial 400 MHz 2D ^{1}H−^{1}H EXSY NMR spectra (mixing time, 50 ms; d_3-acetonitrile, 298 K) showing cross-peaks due to chemical exchange between free $[Co_8L_{12}][BF_4]_{16}$ and the complex $[Co_8L_{12}][BF_4]_{16}$·**19**. Concentrations: $[Co_8L_{12}][BF_4]_{16}$, 0.2 mM; **19**, 10 mM.

The series of NMR spectra in Figure 10 show that the free and bound host signals are in fast exchange for **19**, **29**, and **34** but are in slow exchange with guests **30** and **31**. Thus, guests **30** and **31** (Figure 10, spectra f and e, respectively) gave two or more host·guest signals to replace each host signal as the complex formed. As with guest **23**, which showed the same behavior, this splitting of the host signals into multiple components on guest binding is an indicator of a slow exchange process *within* the host·guest complex, with two or more binding orientations of the guest interconverting slowly on the ^{1}H NMR chemical shift timescale. ^{1}H−^{1}H EXSY NMR experiments on the complex $[Co_8L_{12}][BF_4]_{16}$·**23** again show exchange peaks (Figure 14), but now, these correspond to exchange between different confomers of the host/guest complex. As compared to the situation with guest **19**, the tumbling of guest **23** has slowed down to the extent that this exchange process now lies in the EXSY lifetime window.

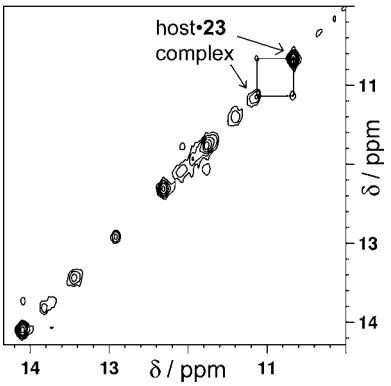

Figure 14. Observation of bound host/bound host exchange in a complex with a slowly tumbling guest. Partial 400 MHz 2D ^{1}H−^{1}H EXSY NMR spectra (mixing time = 50 ms; d_3-acetonitrile, 298 K) showing cross-peaks due to chemical exchange between different conformers of the complex $[Co_8L_{12}][BF_4]_{16}$·**23**. Concentration of $[Co_8L_{12}][BF_4]_{16}$ = 0.2 mM and **23** = 50 mM.

Accordingly, ^{1}H NMR spectroscopy allows the two different dynamic processes involved in binding of the guests inside the cage (exchange between free and bound states, i.e., guest exchange into/out of the cavity; and exchange between different bound states, i.e., tumbling within the cavity) to be observed by EXSY spectroscopy when they fall within the time-scale window provided by this technique. The rates of these two processes therefore affect the appearance of both the 1D spectra (slow or fast exchange on the *chemical shift* timescale) and the appearance of cross-peaks in the EXSY spectra (slow or fast exchange on the *mixing* timescale). This leads to four different time-scale regimes, as summarized in Figure 15: (a) Both exchange processes are fast on both timescales, and the rate of neither can be measured ($t_{1/2} < 10^{-2}$ s for both). (b)

dx.doi.org/10.1021/ic302498t | Inorg. Chem. 2013, 52, 1122−1132

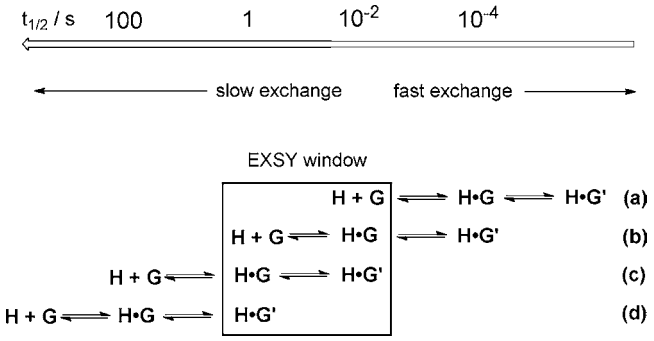

Figure 15. Correlation of the timescales of different dynamic processes with the window allowed by EXSY measurements. H and G denote free host and guest; H·G and H·G′ denote different conformers of the bound complex.

Exchange between free and bound states is slow on the chemical shift timescale and fast on the mixing timescale. Exchange between different bound states is fast on both timescales. Under these conditions, limits on the rate of exchange *between free and bound states* can be measured ($1\ s < t_{1/2} < 10^{-2}\ s$); this corresponds to the situation in Figures 4 and 13 with guest **19**. Another example of an EXSY spectrum showing this behavior is in Figure S6 in the Supporting Information for guest **20**. (c) Exchange between free and bound states is slow on both timescales. Exchange between different bound states is slow on the chemical shift timescale but fast on the EXSY mixing timescale. Under these conditions, limits on the rate of exchange *between different bound states* can be measured ($1\ s < t_{1/2} < 10^{-2}\ s$); this corresponds to the situation in Figure 14 with guest **23**. Another example of an EXSY spectrum showing this behavior is in Figure S7 in the Supporting Information for guest **30**. (d) Both exchange processes are slow on both timescales, and the rate of neither can be measured ($t_{1/2} > 1$ s for both).

For the smaller monocyclic guests **25**, **26**, **27**, and **28** (see Figure 5), the exchange between free and bound states is fast on the chemical shift timescale because diffusion through the portals in the cage is relatively unhindered. For the larger bicyclic guest molecules such as **19**–**23** (Figure 5), the exchange between free and bound states is slow on the chemical shift timescale for both host and guest signals, because these compounds do not fit through the portals in the cage without some distortion, which leads to a larger activation barrier. Guests **19** and **20** show chemical exchange cross-peaks between the free and the bound cage in the EXSY spectrum (Figures 13 and S6 in the Supporting Information), and using the integrals of the cross-peaks, it is possible to estimate the exchange rates to be 29–36 s^{-1} for **19** and 17–19 s^{-1} for **20**.[19] For guests that have exchangeable OH or NH protons (**21**, **22**, **29**, and **34**), the bound ^{1}H NMR signals are relatively broad, presumably due to exchange of the NH and OH protons, and no cross-peaks are observed in the EXSY spectra.

With guests **23**, **30**, and **31**, no cross-peaks are observed between free and bound signals in the EXSY spectra. The additional steric bulk conferred by the substituents on **30** and **31** makes passage through the portals in the cage more difficult for these guests than for the parent compound **19**, and this reduces the rate of exchange between free and bound states to below the EXSY detection limit. Guest **23** is isosteric with **19** and **20**, but it has a significantly higher association constant, and this is sufficient to reduce the rate of exchange between free and bound states below the EXSY detection limit. Thus, the activation barrier to guest release is a function of both binding affinity and steric complementarity with the portals.

For guests **23** (Figure 14) and **30** (Figure S7 in the Supporting Information), slow exchange between signals due to *two different bound states* is observed on the chemical shift timescale, and EXSY cross-peaks are observed between these signals. Using the integrals of the cross-peaks, it is possible to estimate the exchange rates as 1.0–5.5 s^{-1} for **23** and 2.2–13 s^{-1} for **30**. In the case of **30**, the steric bulk of the additional C^4 substituent presumably hinders rotation of the guest within the cavity, leading to slow exchange between bound states, but for **23**, the reasons are less obvious. Guest **23** makes the strongest H-bonding interactions with the cage among the ones that we have investigated, and the slow exchange observed between different bound states suggests that these H-bonds have to be broken for the guest to change its orientation inside the cavity.

The ^{1}H NMR spectrum for the complex formed with guest **31** is the most complicated with slow exchange between multiple bound host signals (Figure 10, spectrum e). In this case, no cross-peaks are observed in the EXSY spectrum, which indicates that exchange between free and bound states *and* between the multiple bound orientations of the guest are all slow on the EXSY timescale. This is the largest guest, and the size of the C^4 substituent and its "docking" with a portal in the cage surface (Figure 12) apparently creates a large steric barrier to rotation of the guest within the cavity.

■ CONCLUSIONS

The $[Co_8L_{12}]^{16+}$ cage acts as a remarkably size- and shape-selective host for small organic guests such as coumarin (**19**) and other bicyclic molecules of comparable size and shape. We have been able to exploit the paramagnetism of the host cage, which disperses the ^{1}H NMR signals over a range of ca. 200 ppm, to facilitate detailed analysis of the strengths of and the factors responsible for, guest binding, and the dynamic behavior of the guest in the cavity. The highest affinity guest is isoquinoline-*N*-oxide (**23**) with $K = 2100\ M^{-1}$ in acetonitrile.

Two types of recognition element are independently involved in guest binding. The first is a hydrogen bond-accepting carbonyl or *N*-oxide group, which interacts with one of two binding sites inside the cage associated with the *fac* tris-chelate vertices; these sites combine a convergent set of CH groups as H-bond donors, with high positive electrostatic potential due to proximity to the metal centers. The magnitude of this contribution to the binding free energy varies linearly with the β-parameter, which describes the H-bond accepting ability of the O atom. The H-bond donor ability of the cage is considerable, with an α value similar to that of phenol. The second recognition element is the additional aromatic ring, which contributes a fixed amount of ca. 10 kJ/mol to the free energy of binding via favorable interactions with the interior surface of the host cage and/or solvophobic interactions. Addition of small substituents at many sites on the coumarin-based guests completely removes their ability to bind, indicating strong size/shape selectivity. However, the coumarin-type guests can accommodate Me or OMe substituents at the C^4 position whose additional bulk results in slower exchange between free/bound guests and also slower reorientation of the guest inside the cavity, as shown by conventional ^{1}H NMR and also ^{1}H–^{1}H EXSY spectroscopy. Having identified the recognition elements necessary for good

dx.doi.org/10.1021/ic302498t | *Inorg. Chem.* 2013, 52, 1122–1132

guest binding, we are now in a position to design new guests that exploit these recognition features optimally.

EXPERIMENTAL SECTION

Syntheses. The host cage $[Co_8L_{12}]X_{16}$ (X = perchlorate or tetrafluoroborate) was prepared as previously described[10,12] and crystallized before use; the identity and purity of every batch were confirmed by ^{1}H NMR spectroscopy. $[Co_8L_{12}](BPh_4)_{16}$ was prepared by stirring a mixture of $Co(CH_3CO_2)_2{\cdot}6H_2O$ (0.019 g, 0.075 mmol) and L (0.050 g, 0.113 mmol) in MeOH for 1 h to give a clear solution; the addition of aqueous $NaBPh_4$ (0.052 g, 0.151 mmol) afforded a pink precipitate, which was filtered off, washed with MeOH, dried, and crystallized by diffusion of ethyl acetate vapor into a solution of the complex in $MeNO_2$ (yield, 55%). The identity of the cage was confirmed by ES mass spectrometry and ^{1}H NMR spectroscopy, which gave results essentially identical to those reported earlier for the other salts. Syntheses of guest molecules 4-methyl-coumarin (**30**, modified from a literature preparation)[18] and **4** are described in the Supporting Information.

X-ray Crystallography. A crystal of $[Co_8L_{12}](BPh_4)_{16}$ grown from $MeNO_2$/ethyl acetate (orange block) was mounted on a Bruker APEX-2 diffractometer under a stream of cold N_2. Details of crystal parameters, data collection, and refinement are collected in Table 4.

Table 4. Crystal Parameters, Data Collection, and Refinement Details for the Structural Determination of $[Co_8L_{12}](BPh_4)_{16}$

formula	$C_{720}H_{584}B_{16}Co_8N_{72}$
formula weight	10888.99
T (K)	110(2)
l (Å)	0.71073
crystal system	rhombohedral
space group	$R\bar{3}$
a (Å)	31.1071(6)
c (Å)	54.3615(10)
V (Å^3)	45555.5(15)
Z	3
D_{calcd} (Mg/m^3)	1.191
μ (mm^{-1})	0.278
data, restraints, parameters	13270, 54, 913
R_{int} for independent data	0.1020
final R_1, wR_2	0.0948, 0.2970

Data were collected at 110 K using Mo Kα radiation from a conventional sealed-tube source. After integration of the raw data and before merging of symmetry equivalents, an empirical absorption correction was applied (SADABS).[20] The structure was solved by direct methods and refined using the SHELX suite of programs.[21] The crystals scattered weakly due to disorder of anions and solvent molecules, and the refinement required extensive use of geometric and displacement restraints (detailed in the CIF). The molecule lies on a crystallographic S_6 axis such that one-sixth of it is unique. Thus, the asymmetric unit contains one metal ion in a general position [Co(1)] and one on a 3-fold axis [Co(2)], two complete ligands, and two complete anions. Large areas of diffuse electron density that could not be modeled sensibly were eliminated from the refinements using the SQUEEZE function in PLATON;[22] details are in the CIF. The final R_1 value of 9.5% is good for a cage complex of this type.

NMR Titrations. NMR titrations were carried out on a Bruker Avance-III 400 MHz instrument at 298 K. A 10 mL sample of the host cage complex (tetrafluoroborate salt) was prepared at a known concentration (0.13−0.3 mM) in CD_3CN. A 5 mL solution of guest (0.5−1000 mM) was prepared using the host solution, so that the concentration of host remained constant throughout the titration. Increasing aliquots of guest solution were added to 12 NMR tubes and made up to 0.6 mL with host solution. The NMR spectrum was recorded for each sample. Changes in chemical shifts or peak areas were analyzed by using the appropriate binding isotherms in Microsoft Excel. Each titration was repeated at least three times, and the experimental error is quoted as twice the standard deviation at a precision of one significant figure.

Computational Studies. The electrostatic potential was obtained from the wave function from a single-point DFT calculation using the B3LYP functional.[23] This calculation was performed using Gaussian 09, version C.02,[24] compiled using Portland compiler v 8.0-6 with the Gaussian-supplied versions of ATLAS and BLAS.[25] We used a Stuttgart/Dresden pseudo potential on Co[26] and D95 V on all other atoms (Keyword SDD in G09).[27] Our calculation contained 5000 basis functions and 2904 electrons. No symmetry was taken into account, and we did not include the role of the solvent, instead performing the calculations in vacuo. The starting point for the SCF cycle was generated using "guess=indo". Visualization was done using the CCP1-GUI.[28]

The large number of basis functions and electrons means that this calculation was time-consuming and slow to converge. Therefore, we stopped the calculation when the energy had converged to 8×10^{-6}, which was achieved after 111 iterations. The molecular mechanics calculations of host/guest complex structures were performed using the software in ref 29.

ASSOCIATED CONTENT

Supporting Information

Additional views of the structure of $[Co_8L_{12}](BPh_4)_{16}$ showing the interaction of the anion with the cage exterior surface; synthesis of compounds **4** and **30**; additional ^{1}H NMR data and ^{1}H−^{1}H EXSY spectra for cage complexes with guests **20** and **30**. This material is available free of charge via the Internet at http://pubs.acs.org.

AUTHOR INFORMATION

Corresponding Author

*E-mail: c.hunter@sheffield.ac.uk (C.A.H.) or m.d.ward@sheffield.ac.uk (M.D.W.).

Notes

The authors declare no competing financial interest.

ACKNOWLEDGMENTS

We thank the EPSRC for funding and Dr. Brian Taylor for assistance with the NMR spectroscopic measurements.

REFERENCES

(1) Reviews on coordination cages: (a) Fiedler, D.; Leung, D. H.; Bergman, R. G.; Raymond, K. N. *Acc. Chem. Res.* **2005**, *38*, 349. (b) Fujita, M.; Tominaga, M.; Hori, A.; Therrien, B. *Acc. Chem. Res.* **2005**, *38*, 369. (c) Seidel, S. R.; Stang, P. J. *Acc. Chem. Res.* **2002**, *35*, 972. (d) Hamilton, T. D.; MacGillivray, L. R. *Cryst. Growth Des.* **2004**, *4*, 419. (e) Ward, M. D. *Chem. Commun.* **2009**, 4487. (f) Perry, J. J.; Perman, J. A.; Zaworotko, M. J. *Chem. Soc. Rev.* **2009**, *38*, 1400. (g) Alvarez, S. *Dalton Trans.* **2006**, 2209. (h) Amouri, H.; Desmarets, C.; Moussa, J. *Chem. Rev.* **2012**, *112*, 2015. (i) Williams, A. F. *Coord. Chem. Rev.* **2011**, *255*, 2104. (j) Laughrey, Z.; Gibb, B. *Chem. Soc. Rev.* **2011**, *40*, 363. (k) Jin, P.; Dalgarno, S. J.; Atwood, J. L. *Coord. Chem. Rev.* **2012**, *254*, 1760. (l) Chakrabarty, R. J.; Mukherjee, P. S.; Stang, P. J. *Chem. Rev.* **2011**, *111*, 6810. (m) Inokuma, Y.; Kawano, M.; Fujita, M. *Nature Chem.* **2011**, *3*, 349. (n) Pluth, M. D.; Bergman, R. G.; Raymond, K. N. *Acc. Chem. Res.* **2009**, *42*, 1650. (o) Breiner, B.; Clegg, J. K.; Nitschke, J. R. *Chem. Sci.* **2011**, *2*, 51.

(2) Reviews on organic capsules: (a) Rebek, J. *Acc. Chem. Res.* **2009**, *42*, 1660. (b) Cram, D. J. *Angew. Chem., Int. Ed. Engl.* **1988**, *27*, 1009. (c) Rieth, S.; Hermann, K.; Wang, B.-Y.; Badjić, J. *Chem. Soc. Rev.* **2011**, *40*, 1609. (d) Hof, F.; Craig, S. L.; Nucjolls, C.; Rebek, J. *Angew. Chem., Int. Ed.* **2002**, *41*, 1488. (e) Hooley, R. J.; Rebek, J. *Chem. Biol.*

2009, *16*, 255. (f) Purse, B. W.; Rebek, J. *Proc. Natl. Acad. Sci. U.S.A.* **2005**, *102*, 10777. (g) Cram, D. J. *Nature* **1992**, *356*, 29.
(3) Cram, D. J.; Tanner, M. E.; Thomas, R. *Angew. Chem., Int. Ed. Engl.* **1991**, *30*, 1024.
(4) Mal, P.; Breiner, B.; Rissanen, K.; Nitschke, J. R. *Science* **2009**, *324*, 1697.
(5) Yoshizawa, M.; Tamura, M.; Fujita, M. *Science* **2006**, *312*, 251.
(6) Hastings, C. J.; Pluth, M. D.; Bergman, R. G.; Raymond, K. N. *J. Am. Chem. Soc.* **2010**, *132*, 6938.
(7) (a) Ams, M. R.; Ajami, D.; Craig, S. L.; Yang, J. S.; Rebek, J. *J. Am. Chem. Soc.* **2009**, *131*, 13190. (b) Mecozzi, S.; Rebek, J. *Chem.—Eur. J.* **1998**, *4*, 1016.
(8) Lewis, J. E. M.; Gavey, E. L.; Cameron, S. A.; Crowley, J. D. *Chem. Sci.* **2012**, *3*, 778.
(9) Tashiro, S.; Tominaga, M.; Kawano, M.; Therrien, B.; Ozeki, T.; Fujita, M. *J. Am. Chem. Soc.* **2005**, *127*, 4546.
(10) Tidmarsh, I. S.; Faust, T. B.; Adams, H.; Harding., L. P.; Russo, L.; Clegg, W.; Ward, M. D. *J. Am. Chem. Soc.* **2008**, *130*, 15167.
(11) (a) Stephenson, A.; Argent, S. P.; Riis-Johannessen, T.; Tidmarsh, I. S.; Ward, M. D. *J. Am. Chem. Soc.* **2011**, *133*, 858. (b) Najar, A. M.; Tidmarsh, I. S.; Adams, H.; Ward, M. D. *Inorg. Chem.* **2009**, *48*, 11871. (c) Stephenson, A.; Ward, M. D. *Dalton Trans.* **2011**, *40*, 10360.
(12) Turega, S.; Whitehead, M.; Hall, B. R.; Haddow, M. F.; Hunter, C. A.; Ward, M. D. *Chem. Commun.* **2012**, *48*, 2752.
(13) (a) De Greef, T. F. A.; Smulders, M. M. J.; Wolffs, M.; Schenning, A. P. H. J.; Sijbesma, R. P.; Meijer, E. W. *Chem. Rev.* **2009**, *109*, 5687. (b) Baldridge, K. K.; Cozzi, F.; Siegel, J. S. *Angew. Chem., Int. Ed.* **2012**, *51*, 2903. (c) Ponnuswamy, N.; Pantos, G. D.; Smulders, M. M. J.; Sanders, J. K. M. *J. Am. Chem. Soc.* **2012**, *134*, 566.
(14) Lehn, J.-M.; Eliseev, A. V. *Science* **2001**, *291*, 2331.
(15) (a) Amouri, H.; Mimassi, L.; Rager, M. N.; Mann, B. E.; Guyard-Duhayon, C.; Raehm, L. *Angew. Chem., Int. Ed.* **2005**, *44*, 4543. (b) Tidmarsh, I. S.; Taylor, B. F.; Hardie, M. J.; Russo, L.; Clegg, W.; Ward, M. D. *New J. Chem.* **2009**, *33*, 366.
(16) (a) Hall, B. R.; Manck, L. E.; Tidmarsh, I. S.; Stephenson, A.; Taylor, B. F.; Blaikie, E. J.; Vander Griend, D. A.; Ward, M. D. *Dalton Trans.* **2011**, *40*, 12132. (b) Paul, R. L.; Couchman, S. M.; Jeffery, J. C.; McCleverty, J. A.; Reeves, Z. R.; Ward, M. D. *J. Chem. Soc., Dalton Trans.* **2000**, 845.
(17) (a) Hunter, C. A. *Angew. Chem., Int. Ed.* **2004**, *43*, 5310. (b) Abraham, M. H.; Platts, J. A. *J. Org. Chem.* **2001**, *66*, 3484. (c) Abraham, M. H.; Grellier, P. L.; Prior, D. V.; Morris, J. J.; Taylor, P. J. *Perkin Trans. 2* **1990**, 521. (d) Ajami, D.; Dube, H.; Rebek, J., Jr. *J. Am. Chem. Soc.* **2011**, *133*, 9689. (e) Ajami, D.; Tolstoy, P. M.; Dube, H.; Odermatt, S.; Koeppe, B.; Guo, J.; Limbach, H.-H.; Rebek, J., Jr. *Angew. Chem., Int. Ed.* **2011**, *50*, 528. (f) Jiang, W.; Tieffenbacher, K.; Ajami, D.; Rebek, J. *Chem. Sci.* **2012**, *3*, 3022−3025. (g) Sawada, T.; Fujita, M. *J. Am. Chem. Soc.* **2010**, *132*, 7194.
(18) Woodruff, E. H. *Org. Synth.* **1944**, *24*, 69.
(19) (a) Lu, J.; Ma, D. J.; Hu, J.; Tang, W. X.; Zhu, D. X. *J. Chem. Soc., Dalton Trans.* **1998**, 2267. (b) Perrin, C. L.; Dwyer, T. J. *Chem. Rev.* **1990**, *90*, 935. (c) Pluth, M. D.; Raymond, K. N. *Chem. Soc. Rev.* **2007**, *36*, 161. (d) Pons, M.; Millet, O. *Prog. Nucl. Magn. Reson. Spectrosc.* **2001**, *38*, 267. (e) Mugridge, J. S.; Szigethy, G.; Bergman, R. G.; Raymond, K. N. *J. Am. Chem. Soc.* **2010**, *132*, 16256.
(20) Sheldrick, G. M. *SADABS: A Program for Absorption Correction with the Siemens SMART System*; University of Gottingen: Germany, 1996.
(21) Sheldrick, G. M. *Acta Crystallogr., Sect. A* **2008**, *64*, 112.
(22) Spek, A. L. *J. Appl. Crystallogr.* **2003**, *36*, 7.
(23) Becke, A. D. *J. Chem. Phys.* **1993**, *98*, 5648.
(24) Frisch, M. J.; Trucks, G. W.; Schlegel, H. B.; Scuseria, G. E.; Robb, M. A.; Cheeseman, J. R.; Scalmani, G.; Barone, V.; Mennucci, B.; Petersson, G. A.; Nakatsuji, H.; Caricato, M.; Li, X.; Hratchian, H. P.; Izmaylov, A. F.; Bloino, J.; Zheng, G.; Sonnenberg, J. L.; Hada, M.; Ehara, M.; Toyota, K.; Fukuda, R.; Hasegawa, J.; Ishida, M.; Nakajima, T.; Honda, Y.; Kitao, O.; Nakai, H.; Vreven, T.; Montgomery, J. A., Jr.; Peralta, J. E.; Ogliaro, F.; Bearpark, M.; Heyd, J. J.; Brothers, E.; Kudin, K. N.; Staroverov, V. N.; Kobayashi, R.; Normand, J.; Raghavachari, K.; Rendell, A.; Burant, J. C.; Iyengar, S. S.; Tomasi, J.; Cossi, M.; Rega, N.; Millam, J. M.; Klene, M.; Knox, J. E.; Cross, J. B.; Bakken, V.; Adamo, C.; Jaramillo, J.; Gomperts, R.; Stratmann, R. E.; Yazyev, O.; Austin, A. J.; Cammi, R.; Pomelli, C.; Ochterski, J. W.; Martin, R. L.; Morokuma, K.; Zakrzewski, V. G.; Voth, G. A.; Salvador, P.; Dannenberg, J. J.; Dapprich, S.; Daniels, A. D.; Farkas, O.; Foresman, J. B.; Ortiz, J. V.; Cioslowski, J.; Fox, D. J. *Gaussian 09*, revision C.2; Gaussian, Inc.: Wallingford, CT, 2009.
(25) (a) Whaley, R. C.; Petitet, A. *Software: Practice and Experience* **2005**, *35*, 10. (b) Whaley, R. C.; Petitet, A.; Dongarra, J. J. *Parallel Comput.* **2001**, *27*, 3.
(26) (a) Nicklass, A.; Dolg, M.; Stoll, H.; Preuss, H. *J. Chem. Phys.* **1995**, *102*, 8942. (b) Cao, X. Y.; Dolg, M. *J. Chem. Phys.* **2001**, *115*, 7348 and references therein.
(27) Dunning, T. H., Jr.; Hay, P. J. In *Modern Theoretical Chemistry*; Schaefer, H. F., III, Ed.; Plenum: New York, 1976; Vol. 3, p 1.
(28) Thomas, J.; Sherwood, P. *CCP1-GUI, A General-Purpose Visualization Code for Electronic Structure Codes*, version 0.8; obtained from http://sourceforge.net/projects/ccp1gui (last accessed August. 2012).
(29) *MMFF, MacroModel*, version 9; Schrödinger, Inc.: New York, NY, 2011.